2024 European Control Conference (ECC)
June 25-28, 2024. Stockholm, Sweden

COMPARISON BETWEEN SEVERAL CONTROL TECHNIQUES FOR TUNNELING CURRENT REGULATION

Rafael Correa[1], Alina Voda[1], Gildas Besançon[1]

Abstract— **This paper is about feedback control system for Scanning Tunneling Microscopy (STM). The system aims to maintain a constant tunneling current between tip and sample surface, despite external disturbances. Four controllers are tested and compared, resuming three previously considered techniques, and including a novel genetic-algorithm-based approach. Results in particular highlight the effectiveness of the latter in maintaining stability and rejecting disturbances, and the study includes both simulation and experimental results. The findings hence contribute to the development of reliable control systems for nanoscale imaging and manipulation.**

I. INTRODUCTION

The invention of the Scanning Tunneling Microscope (STM) by Gerd Binnig and Heinrich Rohrer in 1986 marked a significant milestone in nanoscience [1]. This breakthrough technology exploits the quantum mechanical phenomenon of tunneling current, whereby an electron can traverse a potential barrier with a non-zero probability [2]. By positioning an ultra-sharp metallic tip in close proximity to a conductive sample surface, the STM allows for the imaging and characterization of surface morphology at the atomic scale [3]. The success of the STM led to the development of various Scanning Probe Microscopes (SPMs), with the Atomic Force Microscope (AFM) receiving particular attention [4], [5].

The use of tunneling current extends beyond imaging applications, and it has, for instance, proven valuable in measuring submicro-g accelerations [6] or in detecting submicrometer displacements [7]. Achieving accurate tunneling effects requires ultrahigh positioning accuracy and high bandwidth, presenting significant challenges in control system design. The control scheme typically includes a tunneling current sensor, a regulation feedback loop, and a piezoelectric actuator for precise tip movement (see Figure 1). While commercial SPMs often employ simple control strategies such as Proportional-Integral (PI) controllers with manual tuning, the scientific community has made notable advances in control problems for SPMs over the past decades [8], particularly AFMs (see, e.g., [9] and references therein), but also STMs [10], [11], [12], [13], [14], [15].

In this specific case of STM, a precise information on tunneling current is crucial for achieving accurate imaging and characterization of surfaces. However, the presence of various noise sources [16] as well as unknown sample surface variations greatly impact the precision of tunneling current measurements. Moreover, nonlinearities and physical limitations within the control loop can raise significant challenges and limit system performance in practice. This motivates for a special care on advanced control strategies specifically tailored to tunneling phenomena.

In such a context, and on the basis of the experimental STM-like setup developed by the control group at GIPSA-lab [17], our purpose in this paper is to compare various possible approaches for the control of tunneling current under piezoelectric actuation and current sensing: four control techniques have been chosen, including a standard Proportional Integral (PI) regulator, two methods coming from former works of the Gipsa control group towards *robust* designs (one based on combined pole placement with sensitivity function shaping as in [18], and the other one based on H_∞ technique as in [19]), and one new approach based on Genetic Algorithm.

The main objective is to compare the performance and effectiveness of these controllers in terms of their ability to maintain the desired tunneling current and reject external disturbances. The controllers are evaluated based on criteria such as tracking accuracy, robustness, and sensitivity to noise, and compared on the basis of simulation as well as experimental results.

The system modelling is first presented in section II and considered controllers are displayed in section III. Simulation results are then given in section IV, with experimental ones in section V. Some conclusions end the paper in section VI.

II. SYSTEM DESCRIPTION AND MODELING

A. Principle of operation

The Scanning Tunneling Microscope (STM) operates based on a fundamental principle: measurement and control of the tunneling current (i_t) that appears between a sharp metallic tip and a sample surface under some bias voltage (v_b). This process occurs when the tip and the surface are positioned at a distance (d) smaller than 1×10^{-9} m. The tunneling current then exponentially depends on the distance between the tip and the surface, according to:

$$i_t(t) = g \cdot v_b \cdot e^{-k \cdot d(t)} \tag{1}$$

In this equation, g and k are constants determined by the work functions of the tip and the sample surface, respectively. The primary objective of the feedback control system in the vertical z-direction is to maintain a constant distance (or equivalently, a constant tunneling current) despite the presence of external disturbances such as noise (n) and variations in the sample surface (z_s).

[1]Rafael Correa, Alina Voda and Gildas Besançon are with Univ. Grenoble Alpes, CNRS, Grenoble INP*, GIPSA-lab, 38000 Grenoble, France. {rafael.do-amaral-correa, alina.voda, gildas.besancon}@gipsa-lab.grenoble-inp.fr
*Institute of Engineering Univ. Grenoble Alpes

To achieve this, the system employs a closed-loop control scheme, as depicted in Figure 1. A feedback loop continuously monitors tunneling current i_t, transformed into measurable voltage (v_3) by a (high gain) current-to-voltage converter (CVC). However, this voltage is subject to measurement noise (n), resulting in the available feedback voltage (v_y). Simultaneously, a piezoelectric actuator is connected to the tip, enabling precise movement in response to an applied voltage (v_2), after amplification of the control signal (v_1). The position variations of the piezoelectric actuator (z) directly determine the distance $d(t) = d_0 + z_s(t) - z(t)$ (where d_0 represents its initial value).

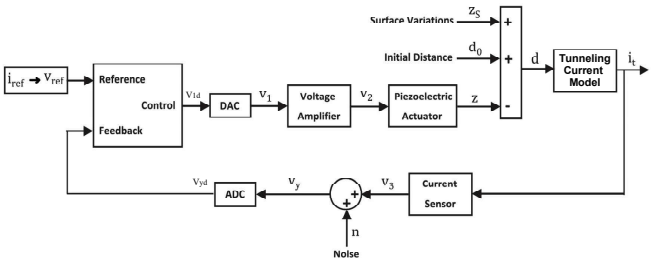

Fig. 1. Complete STM model

Notice that actuator hysteresis can here be neglected in the vertical motion due to the small range of operation [20].

B. Experimental setup

In order to experimentally validate the present study, a setup developed at GIPSA-lab [17] is used (Figure 2).

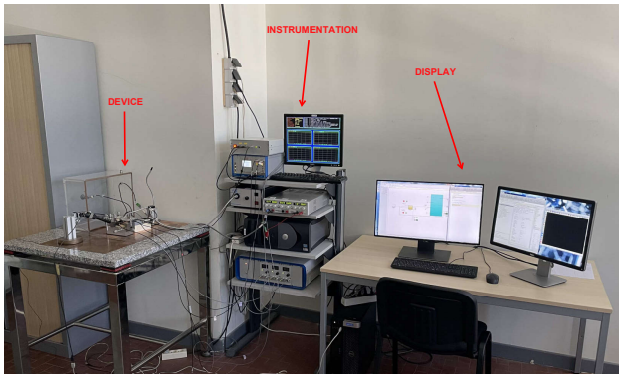

Fig. 2. Experimental platform

This setup uses a tip made of platinum/iridium, and a Piezomechanics/PSt150 actuator. The voltage amplifier is a Piezojena/ENV300, and the CVC is home-made.

The sample surface used in the experiment is graphite, and a camera with telecentric zoom is included to assist the operator in manually positioning the tip prior to closed-loop experiment.

The entire experimental setup is placed on an anti-vibration table (Microworld) to minimize external disturbances, and the control scheme is implemented on a computer system, consisting of a Development PC with a 2.5 GHz processor and a Target PC with a 3.2 GHz processor.

To ensure the integrity of numerical signals and avoid aliasing, an anti-aliasing filter with a bandwidth of 10 kHz is employed, allowing for a sampling frequency of up to 20 kHz. The control algorithms, designed using MATLAB/Simulink^{TM}, are executed on the Target PC and communicated to the experimental setup via Ethernet.

C. Complete model

The complete model of the experimental STM device, as shown in Figure 1, consists of 4 components which can be represented as follows (with all numerical values summarized in Table I):

1) Voltage amplifier:

$$H_{VAz}(s) = \frac{G_{VAz}\omega_{VAz}}{s+\omega_{VAz}} \tag{2}$$

2) Piezoelectric actuator:

$$H_{Piezoz}(s) = \frac{-G_{pz}\omega_{pz}^2}{s^2+2\zeta_{pz}\omega_{pz}s+\omega_{pz}^2} \tag{3}$$

3) Current sensor:

$$H_{CSz}(s) = \frac{G_{CSz}\omega_{CSz}}{s+\omega_{CSz}} \tag{4}$$

4) Tunneling current and linear approximation: Tunneling current i_t is described by Eq. (1), but to facilitate linear control design, a first-order linear approximation is used around an equilibrium value i_{eq}, as:

$$i(t) = i_{\text{eq}} - k_{\text{eq}} \cdot i_{\text{eq}} \cdot (d(t) - d_{\text{eq}}) \tag{5}$$

where d_{eq} represents the corresponding equilibrium distance for a zero equilibrium disturbance z_s.

TABLE I
STM SYSTEM PARAMETERS

Parameters	Value	Unit	Signification
G_{VAz}	15	V/V	Gain of voltage amplifier
ω_{VAz}	4	kHz	Bandwidth of voltage amplifier
G_{pz}	1.2	nm/V	Gain of piezoelectric actuator
ω_{pz}	120	kHz	Bandwidth of piezoelectric actuator
ζ_{pz}	0.9	-	Damping of piezoelectric actuator
G_{CSz}	10^9	V/nA	Gain of current sensor
ω_{CSz}	13	kHz	Bandwidth of current sensor
g	0.0011	-	Tunneling current constant
V_b	1.025	v	Bias voltage
k	16.5	nm^{-1}	Material constant
d_0	1	nm	Initial distance
i_{eq}	1	nA	Equilibrium tunneling current

III. CONSIDERED CONTROLLERS

In this work, four different controllers are considered: a pole-placement controller with sensitivity function shaping, designed as in [18]; an H_∞ controller designed as in [21]; a genetic algorithm-based controller, newly considered in the present work; and a simple PI controller, for comparison. They are all designed according to similar specifications, and with a similar complexity, described in subsection III-A, and all compared in subsequent sections.

A. Control problem formulation and desired performance

Considering an overall discrete-time transfer function of the system (between V_{1d} and V_{yd} in Figure 1) of the form:

$$G(z^{-1}) = z^{-d}\frac{B(z^{-1})}{A(z^{-1})} \tag{6}$$

where d represents the system delay, and z^{-1} stands for the delay operator, the controller to be implemented is searched under a general RS form as:

$$K(z^{-1}) = \frac{R(z^{-1})}{S(z^{-1})} \tag{7}$$

for appropriate polynomials R, S.

About the model, from former identification studies, as in [18], the dynamics of piezoelectric actuator and current sensor can be approximated as constant gains, and the overall model can reduce to $B(z^{-1}) = b_1 z^{-1}, A(z^{-1}) = 1 + a_1 z^{-1}$ with $b_1 = 233.8$, $a_1 = -0.433$, and $d = 1$.

As for the control, its objectives can be summarized as:

1) high measurement accuracy for current control;
2) good robustness and stability margins;
3) large closed-loop bandwidth;
4) noise attenuation at the system input.

Quantitatively, those requirements can be translated into constraints on classical closed-loop sensitivity functions:

• Ouptut sensitivity function (transfer between z_s and i_t):

$$S_0(z^{-1}) = \frac{A(z^{-1})S(z^{-1})}{A(z^{-1})S(z^{-1}) + z^{-d}B(z^{-1})R(z^{-1})} \tag{8}$$

• Input sensitivity function (transfer between n and v_1):

$$K(z^{-1})S_0(z^{-1}) = \frac{A(z^{-1})R(z^{-1})}{A(z^{-1})S(z^{-1}) + z^{-d}B(z^{-1})R(z^{-1})} \tag{9}$$

• Complementary sensitivity function (between n and i_t):

$$T(z^{-1}) = \frac{B(z^{-1})R(z^{-1})}{A(z^{-1})S(z^{-1}) + z^{-d_l}B(z^{-1})R(z^{-1})} \tag{10}$$

as follows:

$$\|S_0(z^{-1})\|_\infty \leq 6\,\text{dB} \tag{11}$$

$$\|T(z^{-1})\|_\infty \leq 3.5\,\text{dB} \tag{12}$$

$$\|K(z^{-1})S_0(z^{-1})\|_\infty \leq 20\,\text{dB} \tag{13}$$

In addition, to enhance measurement accuracy, a maximum variation of $\pm 10\%$ is allowed in the desired tunneling current. This translates into a maximum allowed error voltage v_e, or a lower limit (-20 dB) for sensitivity function $S_0(z^{-1})$, in the measurement bandwidth ω_m (related to expected variations in z_s). The influence of surface variations z_s on the controlled output i_t is given by the transfer function $c_1 \cdot S_0(z^{-1})$, where $c_1 = -k \cdot i_{eq}$. This yields an additional constraint as:

$$|S_0(z^{-1})|_{dB} \leq -27.2\,\text{dB}, \quad 0 \leq \omega \leq \omega_m \tag{14}$$

Furthermore, to limit the influence of noise n on the system input v_1, the transfer function $K(z^{-1})S_0(z^{-1})$ should be restricted, here below 1% of the noise level:

$$|K(z^{-1})S_0(z^{-1})|_{dB} < -40\,\text{dB}, \quad \omega > \omega_m \tag{15}$$

The sampling frequency f_s is set to 20 kHz for all signals, and the desired closed-loop bandwidth to approximately 4 kHz, similar to the voltage amplifier's bandwidth.

B. Controller with pole placement and sensitivity function shaping technique

Let us recall here the design of [18], based on the methodology, e.g. described in [22]:

1) Closed-loop dominant poles: placed at 4 kHz with a damping coefficient of 0.9 to maintain a similar closed-loop natural frequency as the open-loop system.
2) Closed-loop auxiliary poles: a pole added at -0.6 to enhance the robustness of the feedback loop.
3) Controller fixed part in S: an integrator is included.
4) Controller fixed part in R: a real zero is introduced at $0.5 f_s$ to shape the input sensitivity function and open the loop at the Nyquist frequency.

This results in a controller (7) given by:

$$K(z^{-1}) = \frac{0.002 + 0.00117z^{-1} - 0.00083z^{-2}}{1 + 0.15375z^{-1} - 0.7068z^{-2} - 0.44694z^{-3}} \tag{16}$$

C. Controller with H_∞ technique

An H_∞ controller can be obtained according to specifications (11)-(15), for instance as in [21], with templates for sensitivity functions as follows (here expressed in frequency domain):

• Output Sensitivity Function:

$$|S_0(j\omega)| \leq \left|\frac{j\omega + \omega_S\varepsilon_S}{j\omega/M_S + \omega_S}\right|, \quad \forall\omega \tag{17}$$

where, $M_S = 2$ is chosen to provide robustness and stability margins across all frequency ranges, $\omega_S = 1.2 \times 10^4$ rad/sec ensures good disturbance attenuation, and ε_S is set to a very small value to achieve the desired measurement accuracy.

• Input sensitivity function:

$$|KS_0(j\omega)| \leq \left|\frac{\varepsilon_{KS}j\omega + \omega_{KS}}{j\omega + \omega_{KS}/M_u}\right|, \quad \forall\omega \tag{18}$$

where $M_u = 10$ is chosen to impose a limit on the maximum value of the controller output, $\omega_u = 1.88 \times 10^4$ rad/sec, and $\varepsilon_u = 0.5$ to limit the effect of noise (n) at high frequencies in the system input.

• Complementary Sensitivity Function:

$$|T(j\omega)| \leq \left|\frac{\varepsilon_T j\omega + \omega_T}{j\omega + \omega_T/M_T}\right|, \quad \forall\omega \tag{19}$$

where $M_T = 1.5$ is chosen to provide a good robustness margin across all frequency ranges, $\omega_T = 1.88 \times 10^4$ rad/sec to attenuate noise (n) at high frequencies, and $\varepsilon_T = 0.5$.

After computation, a fourth-order controller is obtained. For a fair comparison with the other controllers studied in this work, a model order reduction is applied using a balanced model order reduction algorithm, down to order 3 (as in model (16)). This yields the following controller:

$$K = \frac{0.006328 + 0.0004912z^{-1} - 0.004518z^{-2} + 0.001329z^{-3}}{1 - 0.5236z^{-1} - 0.9856z^{-2} + 0.5093z^{-3}} \tag{20}$$

D. Controller with genetic algorithm

Inspired by the work of [23] for PID tuning, we propose here a Genetic Algorithm (GA) method towards RS tunning, as another possible approach for RS controller design.

Let us recall that GAs draw inspiration from the principles of natural selection and evolution to iteratively evolve a population of potential solutions, aiming to find an optimal or near-optimal solution to a given optimization problem [24].

The GA generally operates on a population of individuals, each representing a potential controller in our context, and the optimization process revolves around a fitness function, which evaluates the quality of each individual (here, controller performances). It is initialized with a random population, and the GA then proceeds through generations, where selection, crossover (recombination), and mutation operations are applied as illustrated in Figure 3.

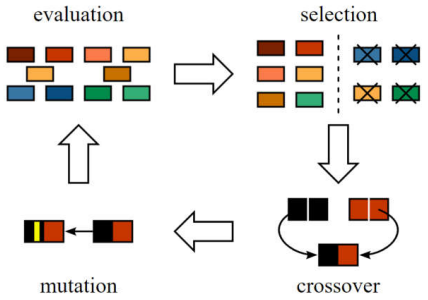

Fig. 3. Genetic algorithm process [25]

The GA iterates until a termination criterion is met (typically when satisfactory performances are reached).

In this work, we consider a controller obtained with MATLAB^{TM}, using a GA that aimed to minimize a cost function based on sensitivity functions and Simulink^{TM} simulations testing the controllers. The simulation operated within a time limit of 0.2 s, with a disturbance of amplitude 0.5 Å and frequency 600 rad/s, together with a reference current of 0.5 nA. The cost function of the GA was defined by weight variables, as shown in Table II, and requirement variables, as shown in Table III.

TABLE II
WEIGHT VARIABLES

Weight 1 (W_1)	Amplitude in dB of $S_0(z^{-1})$ at 600 rad/s
Weight 2 (W_2)	Amplitude in dB of $T(z^{-1})$ at 10 kHz
Weight 3 (W_3)	Amplitude in dB of $T(z^{-1})$ at 5 kHz
Weight 4 (W_4)	Tunneling current values above 0.53 nA
Weight 5 (W_5)	Summed time-weighted absolute error

TABLE III
REQUIREMENT VARIABLES

Requirement 1	Maximum of $S_0(z^{-1})$ should be less than 6 dB
Requirement 2	Maximum of $KS_0(z^{-1})$ should be less than -40 dB
Requirement 3	Maximum of $T(z^{-1})$ should be less than 3.5 dB
Requirement 4	No peaks in tunneling current above 1.5 nA
Requirement 5	i_t value after transient should be less than 0.54 nA
Requirement 6	Controller transfer function should be stable

If one requirement is not met when testing a controller, the cost function is heavily penalized, thus making those criteria limiting. When they are all fulfilled, the cost function reduces to the following (with coefficients heuristically set):

$$J = 10W_1 + 30W_2 + 50W_3 + 10^9 W_4 + 5 \cdot 10^4 W_5 + 200 \quad (21)$$

Notice that the controller to be found was defined with order 3 (for similarity with previous ones), a pole fixed at 1 (to eliminate steady-state error), and a zero fixed at -1 (to open the loop at the Nyquist frequency). Running the genetic algorithm for 40 generations, with 90 individuals per generation, the following controller was obtained:

$$K = \frac{0.0198 + 0.0057z^{-1} - 0.0141z^{-2}}{1 - 0.9427z^{-1} + 0.8285z^{-2} - 0.8858z^{-3}} \quad (22)$$

E. Digital PI controller

Finally, for the sake of comparison, let us recall the digital PI controller also designed in [18], considering the same stability and robustness margins as before:

$$K = \frac{0.00021 + 0.00021z^{-1}}{1 - z^{-1}} \quad (23)$$

IV. SIMULATION RESULTS

This section is dedicated to the comparison of previously presented controllers on the basis of simulations, first based on transfer function models, and then in time domain.

A. Sensitivity functions analysis

Fig. 4 illustrates the Bode diagram of sensitivity functions S_0, KS_0, T, for the 4 controllers, also with SG, representing the relation between system output and input disturbances.

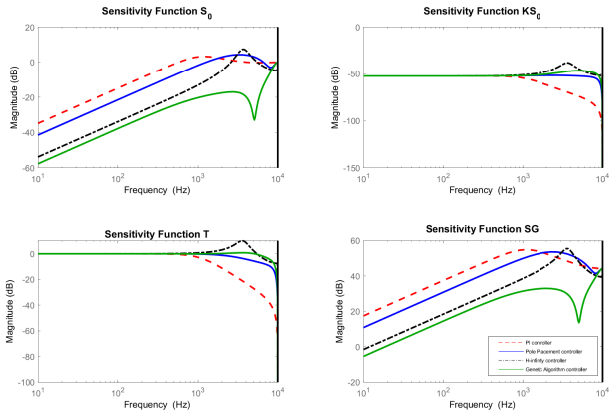

Fig. 4. Bode diagram of sensitivity functions S_0, KS_0, T, and SG (with PI in red, pole placement in blue, H_∞ in black and GA in green)

Starting with output sensitivity function S_0, it can be noticed that all controllers meet the robustness criteria specified in Section III. In addition, it appears that the GA-based controller exhibits superior performance, as it demonstrates lower magnitudes across the entire frequency range. This indicates that it can tolerate higher disturbance frequencies.

About complementary sensitivity function T, it can be seen that the PI controller exhibits the highest tolerance to measurement noise. Furthermore, the H_∞ controller fails to meet the robustness criteria here, as the magnitude of T exceeds 3.5dB in some frequency range. Moreover, it is the only one that does not open the loop at Nyquist frequency.

Finally, examining input sensitivity function KS_0, it can be noticed that all controllers satisfy the robustness criteria of Section III, as the magnitude remains significantly small across all frequencies. This implies that disturbances and noise do not directly interfere with the control signal.

Table IV presents a comparative summary of the closed-loop poles, the frequency where S_0 reaches -27.2 dB, and the frequency where T reaches -3 dB for the four controllers.

B. Time domain simulation

Let us present here simulation results with a model that incorporates actual non-linearities (exponential, saturations), measurement noise (n), and physical limitations in the closed-loop system.

Figure 5 shows the results for the 4 controllers, in the presence of sinusoidal surface variations (z_s) (top graph) with a frequency of 100 rad/s and an amplitude of 0.5 Å. The reference tunneling current is 0.5 nA. It can be observed that the variation in tunneling current remains within the desired limits of 10% with all the designed controllers.

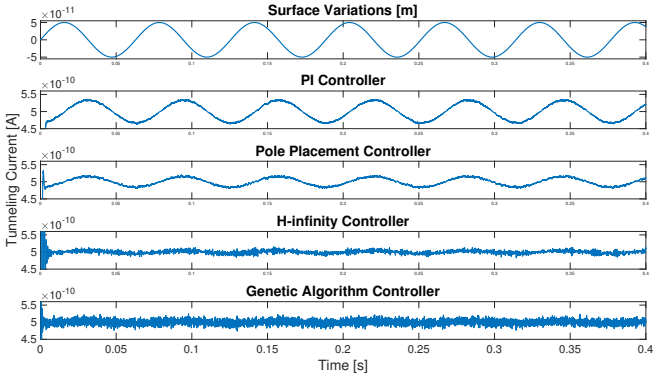

Fig. 5. Simulation results with proposed controllers in the presence of sinusoidal variations (z_s) with frequency of 100 rad/s

However, performances worsen when disturbance frequency is increased, and with 600 rad/s for instance, only GA-based and H_∞ controllers produce acceptable variations in i_t (within the 10% limit), as illustrated by Figure 6.

Notice that all these simulations are performed in the presence of sensor noise (n) with a magnitude of 10 mV/$\sqrt{\text{Hz}}$. In that regard, it can be highlighted that both PI and pole placement controllers exhibit less sensitivity to noise, as observed in the simulation results and sensitivity functions. However, they show inferior performance concerning variations in the tunneling current. On the other hand, GA-based and H_∞ controllers present similar performances, with yet a bit more oscillations in the settling time for the H_∞ controller.

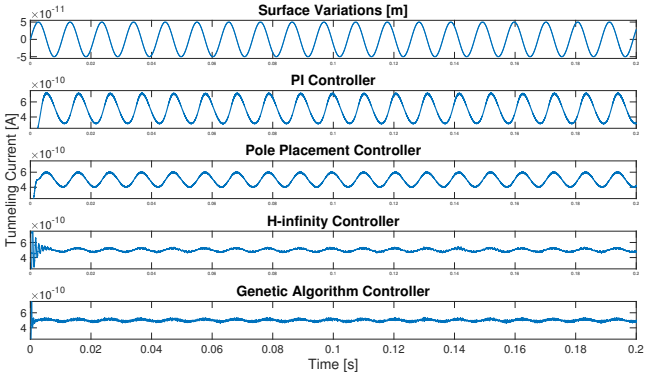

Fig. 6. Simulation results with proposed controllers in the presence of sinusoidal variations (z_s) with frequency of 600 rad/s

V. REAL-TIME EXPERIMENTAL VALIDATION

The effectiveness of the control schemes is further validated through real-time experiments conducted on the experimental platform shown in Figure 2. It is worth noting that the experimental platform operates in an ambient atmosphere, which introduces additional external environmental disturbances beyond those considered in the simulations.

Figures 7 to 10 illustrate the measured tunneling current (i_t) obtained with the 4 controllers. Here, the desired tunneling current is 0.5 nA (corresponding to 0.5 V after CVC).

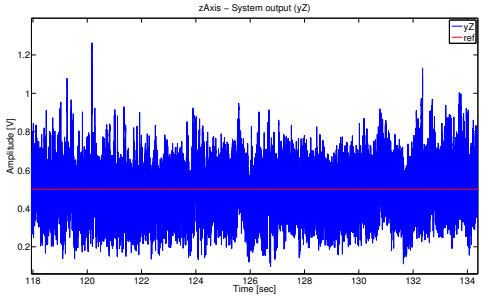

Fig. 7. Measured tunneling current vs its reference with PI controller

The results show that all four tested controllers were capable of maintaining the tunneling current in accordance with the desired reference value. Notably, the GA-based controller exhibited smaller variations in the tunneling current as

TABLE IV
CONTROLLER PERFORMANCE COMPARISON

Controller	Parameters			Complex Poles	
	Closed loop poles	Freq. S_0 = -27.2 dB	Freq. T = -3 dB	ω_n	ζ
PI	0.7571 ± j0.1784 -0.0812	24.2 Hz	1.04 kHz	0.7778	0.9733
Pole Placement	0.4378 ± j0.1649 0.004; -0.6	51.8 Hz	3.22 kHz	0.4678	0.9358
H_∞	0.5165 ± j1.1131 0.5165; 0.4; -0.9949	214 Hz	6.34 kHz	1.2271	0.4209
Genetic Algorithm	0.6462 ± j2.408 0.7267; -0.6433	355 Hz	7.21 kHz	2.4932	0.2592

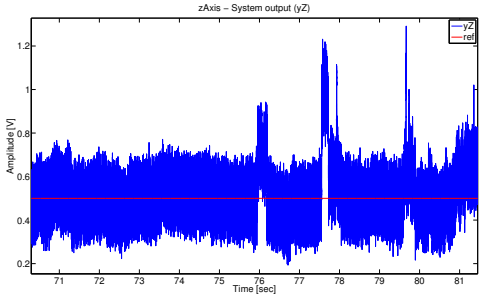

Fig. 8. Measured tunneling current vs its reference with Pole Placement

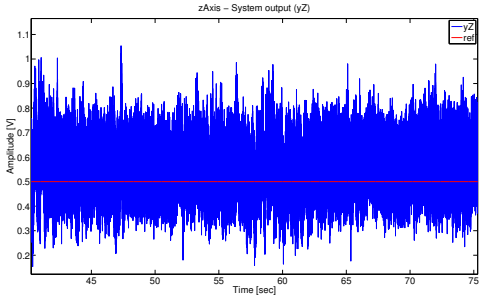

Fig. 9. Measured tunneling current vs its reference with H_∞ controller

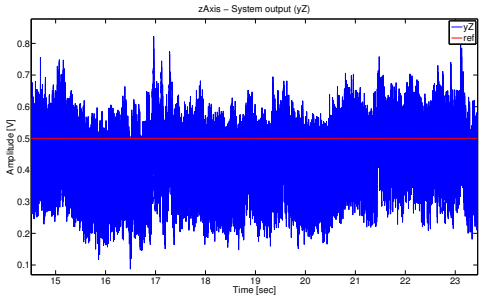

Fig. 10. Measured tunneling current vs its reference with GA controller

compared to the other methods (although with a small bias here), as confirmed by Table V which presents means and variances for the experimental results with each controller.

TABLE V

MEAN AND VARIANCE WITH CURRENT OF 0.5 NA

Controller	Mean Value of Tunneling Current	Variance of Tunneling Current
PI	0.4944	0.0107
Pole Placement	0.5133	0.0112
H_∞	0.5659	0.0077
Genetic Algorithm	0.4268	0.0066

VI. CONCLUSIONS

In conclusion, this work provides a comprehensive study on the design and comparison of four control strategies for precise regulation of tunneling current in scanning tunneling microscopy (STM) systems, aiming at robust and stable performance in the presence of disturbances and uncertainties.

In particular, a new genetic algorithm approach has been proposed for the design of such a controller, which proved to be pretty efficient, both in simulation and experimental tests. The study will be continued by more extensive experiments, and extension to other operation configurations.

REFERENCES

[1] G. Binning and H. Rohrer, "Scanning tunneling microscopy," IBM Journal of Research and Development, 30, 355–369, 1986.

[2] L. D. Landau and E. M. Lifshitz, "Quantum mechanics," Oxford: Pergamon Press, 1977.

[3] C. Julian Chen, "Introduction to Scanning Tunneling Microscopy," Oxford Univ Press, 3rd Ed., 2021.

[4] D. Rugar and P. Hansma, "Atomic force microscopy," Physics Today, 43, 23–30, 1990.

[5] B. Voigtländer, "Atomic force microscopy," Springer , 2nd Ed., 2019.

[6] C. H. Liu, A. M. Barzilai, J. K. Reynolds, A. Partridge, T. W. Kenny, J. D. Grade, et al., "Characterization of a high-sensitivity micromachined tunneling accelerometer with micro-g resolution," Journal of Microelectromechanical Systems, 7(2), 235–244, 1998.

[7] S. Blanvillain, A. Voda, G. Besançon and G. Buche, "The tunnel current as a subnanometer motion sensor," In European control conference. Budapest, Hungary, 2009.

[8] G. Clayton, S. Tien, K. Leang, Q. Zou, and S. Devasia, "A Review of Feedforward Control Approaches in Nanopositioning for High-Speed SPM," ASME Journal of Dynamic Systems Measurement and Control, 131, 10.1115/1.4000158, 2009.

[9] H. Habibullah, "30 Years of atomic force microscopy: Creep, hysteresis, cross-coupling, and vibration problems of piezoelectric tube scanners," Measurement, 159, 2020.

[10] A. Oliva, E. Anguiano, N. Denisenko, M. Aguilar and J. Pena, "Analysis of scanning tunneling microscopy feedback system," Review of Scientific Instruments, 66(5), 3196–3203, 1995.

[11] N. Bonnail, D. Tonneau, F. Jandard, G.-A. Capolino and H. Dallaporta, "Variable structure control of a piezoelectric actuator for a scanning tunneling microscope," IEEE Transactions on Industrial Electronics, 51(2), 354-363, 2004.

[12] I. Ahmad, A. Voda and G. Besancon, "Controller Design for a Closed-Loop Scanning Tunneling Microscope," IEEE International Conference on Automation Science and Engineering, Arlington, VA, USA, pp. 971-976, 2008.

[13] L. Ryba, A. Voda and G. Besançon, "3DOF nanopositioning control of an experimental tunneling current-based platform," IEEE Conference on Control Applications (CCA), Juan Les Antibes, France, pp. 1976-1981, 2014.

[14] F. Tajaddodianfar, S. O. R. Moheimani and J. N. Randall, "Scanning Tunneling Microscope Control: A Self-Tuning PI Controller Based on Online Local Barrier Height Estimation," IEEE Transactions on Control Systems Technology, vol. 27, no. 5, pp. 2004-2015, 2019.

[15] A. Popescu, G. Besançon, A. Voda and S. Basrour, "Observer-Based 3-D Control Enhancement for Topographic Imaging—Validation With an STM Prototype," IEEE Transactions on Control Systems Technology, vol. 29, no. 3, pp. 1075-1086, 2021.

[16] F. Bordoni and M. Karim, "Fundamental noise, electromechanical transduction and their role in resonant gravitational-wave detectors," Classical and Quantum Gravity, 11(6A), 61–72, 1994.

[17] S. Blanvillain, "Contrôle nanoscopique du mouvement par courant tunnel: étude et réalisation," Ph.D. thesis, Univ. Grenoble Alpes, 2010.

[18] I. Ahmad, A. Voda, G. Besançon and G. Buche, "Robust digital control approach for high performance tunneling current measurement system," Control Engineering Practice, 20, 643–653, 2012.

[19] A. Popescu, A. Voda, G. Besançon and Y. Wu, "3D H_∞ Controller Design for an Experimental Scanning Tunneling Microscope Device," 2019 IEEE 58th Conf. Decision & Control, Nice, France, 2019.

[20] N. Bonnail, D. Tonneau, G. A. Capolino and H. Dallaporta, "Dynamic and static responses of a piezoelectric actuator at nanometer scale elongations," In Industry applications conference. Rome, Italy, 2000.

[21] I. Ahmad, A. Voda, G. Besançon and G. Buche, "Tunneling current analysis over an experimental platform with H_∞ control," Journal Européen des Systèmes Automatisés, 45, 507-534, 2012.

[22] I. D. Landau and G. Zito, "Digital control systems: Design, identification and implementation," Springer, 2006.

[23] H. V. H. Ayala and L. S. Coelho, "Tuning of PID controller based on a multiobjective genetic algorithm applied to a robotic manipulator," Expert Systems with Applications, Volume 39, Issue 10, 2012.

[24] J.H. Holland, "Adaptation in Natural and Artificial Systems: An Introductory Analysis with Applications to Biology, Control, and Artificial Intelligence," MIT Press, 1992.

[25] M. Sangiorgio, "A neural approach for multi-reservoir system operation," Master Thesis, Politecnico Milano, Italy, 2016.